Element Selectivity in Second-Harmonic Generation of $GaFeO_3$ by a Soft-X-Ray Free-Electron Laser

Sh. Yamamoto,[1,†] T. Omi,[2] H. Akai,[1] Y. Kubota,[1] Y. Takahashi,[3] Y. Suzuki,[3] Y. Hirata,[1] K. Yamamoto,[1] R. Yukawa,[4] K. Horiba,[4] H. Yumoto,[5] T. Koyama,[5] H. Ohashi,[5] S. Owada,[6] K. Tono,[5] M. Yabashi,[6] E. Shigemasa,[7,8] S. Yamamoto,[1] M. Kotsugi,[3] H. Wadati,[1] H. Kumigashira,[4] T. Arima,[2,9] S. Shin,[1] and I. Matsuda[1,*]

[1]*Institute for Solid State Physics, The University of Tokyo, Kashiwa, Chiba 277-8581, Japan*
[2]*Department of Advanced Materials Science, The University of Tokyo, Kashiwa 277-8561, Japan*
[3]*Tokyo University of Science, Katsushika 125-8585, Japan*
[4]*Photon Factory, Institute of Materials Structure Science, High Energy Accelerator Research Organization (KEK), 1-1 Oho, Tsukuba 305-0801, Japan*
[5]*Japan Synchrotron Radiation Research Institute, Sayo, Hyogo 679-5198, Japan*
[6]*RIKEN SPring-8 Center, Sayo, Hyogo 679-5148, Japan*
[7]*UVSOR Facility, Institute for Molecular Science, Okazaki 444-8585, Japan*
[8]*Sokendai (the Graduate University for Advanced Studies), Okazaki 444- 8585, Japan*
[9]*RIKEN Center for Emergent Matter Science (CEMS), Wako 351-0198, Japan*

(Received 21 October 2017; published 1 June 2018)

Nonlinear optical frequency conversion has been challenged to move down to the extreme ultraviolet and x-ray region. However, the extremely low signals have allowed researchers to only perform transmission experiments of the gas phase or ultrathin films. Here, we report second harmonic generation (SHG) of the reflected beam of a soft x-ray free-electron laser from a solid, which is enhanced by the resonant effect. The observation revealed that the double resonance condition can be met by absorption edges for transition metal oxides in the soft x-ray range, and this suggests that the resonant SHG technique can be applicable to a wide range of materials. We discuss the possibility of element-selective SHG spectroscopy measurements in the soft x-ray range.

DOI: 10.1103/PhysRevLett.120.223902

Nonlinear optical (NLO) frequency conversion, such as second harmonic generation (SHG), is a significant probe to investigate electronic properties, and it has also attracted technological interest of optical control in photonic systems [1–7]. In SHG, optical fields interact with a medium of broken inversion symmetry (IS) to produce a double field frequency. SHG has been used to selectively probe the electronic properties of nonlinear bulk crystals and the interfaces in heterostructures. Recently, the development of a laser in the energy range from extreme ultraviolet to x-ray, the so called free-electron laser (FEL), allows us to explore NLO effects in these energy ranges. All of the earlier studies on nonlinear optics in the hard x-ray range reported experiments conducted under a transmission geometry in order to acquire enough signals by meeting the phase-matching condition [8–13]. In the soft x-ray range, the reflection geometry is preferred because the light in the energy range is strongly absorbed by materials. However, in reflection geometry, the NLO experiments suffer extremely low signals due to the absence of coherent amplification caused by phase matching. A coherent FEL has a much larger intensity than that of conventional light sources in the energy range from extreme ultraviolet (EUV) to hard x-ray, such as synchrotron radiation. This feature of FEL is opening new possibilities for investigating nonlinear optics in this energy region. Furthermore, the SHG spectroscopy using FEL in the soft x-ray range gives element-selective information from a noncentrosymmetric multicomponent system.

In the present study, by using a soft x-ray FEL (SXFEL) [14,15], we demonstrate the observation of SHG from a noncentrosymmetric crystal by employing the FEL and resonance effect described below, even under reflection geometry. SHG signals were detected when the photon energy with double frequency 2ω was above the absorption edge of the sample. The metal M-edge resonance inherently indicates the addition of element specificity to the SHG experiment. Moreover, in the reflection measurement geometry, it is required that the wave vectors along the sample surface be matched, which is automatically satisfied, and the momentum transfer of the sample in the normal direction does not give a critical condition in the regime where the wavelength is larger than the attenuation length. These facts indicate that the present method can be used for various samples and experimental conditions. Experiments of optical frequency conversion with SXFEL are expected to reveal the origins of nonlinear effects in multielement materials and trace the ultrafast dynamics at the interfaces of heterojunctions.

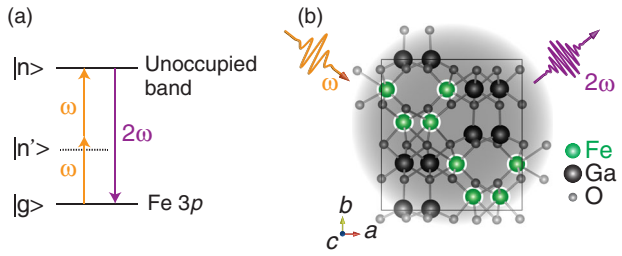

FIG. 1. Second harmonic generation in the $GaFeO_3$ crystal using Fe $3p$ resonance. (a) Energy diagram of SHG. The notations, g, n', and n represent the ground state, intermediate state, and excited state, respectively. (b) Projection view along the c axis of the crystal structure of $GaFeO_3$.

The phenomena of SHG can be expressed in terms of the second-order nonlinear susceptibility $\chi^{\mathrm{SHG}}_{ijk}(2\omega;\omega)$, which becomes zero for centrosymmetric systems in the electric-dipole regime [1,6,16,17]. The value of $\chi^{\mathrm{SHG}}_{ijk}(2\omega;\omega)$ is small with respect to the photon energy, but it can be enhanced when the photon energy $(2\omega;\omega)$ matches with the energy difference of the electronic states of the material [Fig. 1(a)]. With the electric fields $E_j(\omega)$ and $E_k(\omega)$, the SHG $P_i(2\omega)$ is expressed as $P_i(2\omega) = \epsilon_0 \sum_{jk} \chi^{\mathrm{SHG}}_{ijk}(2\omega;\omega) E_j(\omega) E_k(\omega)$. Under the perturbation approximation, $\chi^{\mathrm{SHG}}_{ijk}(2\omega;\omega)$ is simply written as [1]

$$\chi^{\mathrm{SHG}}_{ijk}(2\omega;\omega) = \frac{N}{\epsilon_0 \hbar^2} \sum_{nn'} \left(\frac{\langle i\rangle_{gn} \langle j\rangle_{nn'} \langle k\rangle_{n'g}}{(\omega_{ng} - 2\omega)(\omega_{n'g} - \omega)} + \frac{\langle j\rangle_{gn} \langle i\rangle_{nn'} \langle k\rangle_{n'g}}{(\omega_{ng} + \omega)(\omega_{n'g} - \omega)} + \frac{\langle j\rangle_{gn} \langle k\rangle_{nn'} \langle i\rangle_{n'g}}{(\omega_{ng} + \omega)(\omega_{n'g} + 2\omega)} \right), \quad (1)$$

where $\langle j\rangle_{gn}$ is the jth Cartesian component of the dipole transition matrix element and N is the total atomic or molecular number density. If the target system has the IS, the numerator becomes zero because of parity. The denominators of the first and second terms correspond to the resonance factors. $\chi^{(\mathrm{SHG})}_{(ijk)}(2\omega;\omega)$ becomes large by the condition $2\omega = \omega_{ng}$ or $\omega = \omega_{n'g}$. Thus, if the photon energy of the ultrashort pulse laser can be tuned to the binding energy of the absorption edge in the material, the SHG signal in the soft x-ray range is likely to be enhanced by the resonance effect.

The SHG experiment was performed at the SXFEL beam line (BL1) at the SPring-8 Angstrom Compact free electron Laser (SACLA) in Japan [18]. The FEL was operated at the nominal electron beam energy of 400 MeV in the experiment. A SXFEL was adopted from advantages of tunable photon energy in the EUV-soft x-ray range and in ultrahigh brilliance that allow us to examine nonlinear optics at various photon energy. The SXFEL beam was focused on the sample with a spot size of ~100 μm. The pulse energy at the sample position was determined by a calibrated beam monitor and the calculated reflectivity of the Kirkpatrick–Baez mirror. As a spectrometer, a laminar-type replica diffraction grating with 1200 grooves/mm was used to disperse the photon energy of the reflected light. The reflected light from the sample, which passed through a slit with 200 μm width in the horizontal direction, was incident on the grating at 87°. The diffracted intensity from the grating was measured using a microchannel plate (MCP) detector that could be moved along the energy-dispersion direction. The surface of the MCP detector was coated with CsI to obtain sufficient sensitivity for soft x-ray photons [19,20].

We measured the SHG signal from a single crystal of $GaFeO_3$ [21], which has a noncentrosymmetric orthorhombic structure with space group $Pc2_1n$ at room temperature and is known to show SHG in the visible range [22]. Figure 1(b) shows a projection view of the crystal structure along the c axis with spontaneous polarization along the b axis. The photon energy of the SXFEL pulse was set to half of the Fe $3p$ absorption edge. Thus, the SHG resonance condition $(2\omega = \omega_{ng})$ is satisfied by the energy difference between the Fe $3p$ level and the unoccupied band, as shown in Fig. 1(a). Figure 2(a) shows an overview of the beam line and the measurement system. A FEL beam was generated by the principle of self-amplified spontaneous emission (SASE), which is associated with formation of the microbunching structure of an electron beam. The SXFEL was operated with a repetition rate at 60 Hz. Owing to the SASE scheme, the intensity of the SXFEL pulses fluctuated by 32%. This was evaluated by the coefficient of variation, which was the standard deviation divided by the average. The incident power I_0 was measured using the photoionization of Ar gas at the I_0 monitor in a shot-by-shot manner. With the spectrometer installed at the beam line, we confirmed that the intensity of the second-order harmonics of SXFEL, or spontaneous undulator radiation, was below the detection limit, and it is less than one order of magnitude smaller than the nonlinear signals. The SXFEL pulses with durations of 100 fs and energies of up to 25 μJ were irradiated onto the sample with the p-polarized configuration along the spontaneous polarization axis (b axis) of the $GaFeO_3$ crystal, with an incident angle of 45°. The reflected SXFEL beam, with an angle of 45°, entered into a spectrometer composed of a incident slit, a grating, and a MCP detector. The spectral intensities of the reflected light (I_ω and $I_{2\omega}$) were measured by the MCP position, as shown in Fig. 2(a). Under the fixed MCP position around the energy of second harmonics used in this study, photons with energy bandwidth of ~1 eV enter into the MCP. The intensities of the spectral components ω and 2ω were measured in a shot-by-shot manner with individual I_0 shots. Setting the spectrometer at the 2ω configuration, we confirmed that the photoluminescence

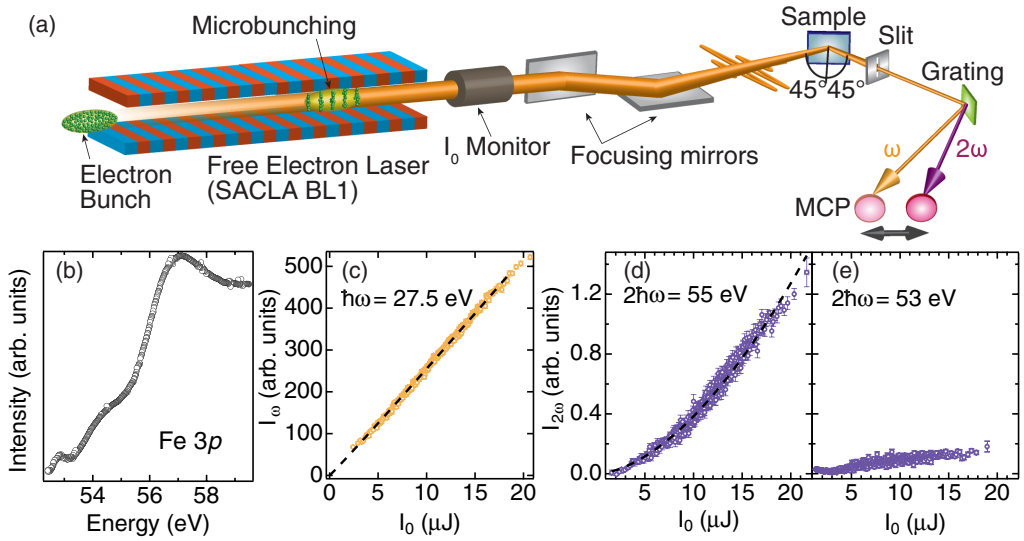

FIG. 2. Measurement of SHG using SXFEL and resonant enhancement of $I_{2\omega}$. (a) Schematic diagram of the SXFEL beam line at SACLA and the SHG measurement system. (b) Fe $3p$ absorption spectrum of the $GaFeO_3$ crystal. (c) Intensity plot of the ω component of the reflected SXFEL pulses I_ω with respect to the correspondent incident intensity I_0 at the photon energy $\hbar\omega = 27.5$ eV. (d) Plot of $I_{2\omega}$ at the photon energy of $2\hbar\omega = 55$ eV. (e) Plot of $I_{2\omega}$ at the photon energy of $2\hbar\omega = 53$ eV. The dashed lines shown in (c) and (d) were fitted by a power law.

light from the sample after the two-photon absorption process [23,24] was below the detection limit. This was confirmed by measuring $I_{2\omega}$ by setting the reflected angle from the sample to the value different from the incident angle.

It is worth noting that the individual measurements of the $I_{2\omega}$–I_0 diagrams in Figs. 2 and 3 were performed without artificial regulation of the I_0 intensity, and they were completed after several minutes. The inherent intensity fluctuation of SXFEL allows the experimenters to automatically obtain data, which makes the SHG measurements using SXFEL efficient given the limited beam time.

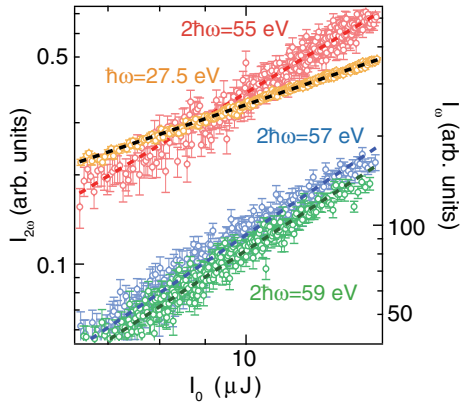

FIG. 3. Quadratic dependence of the $I_{2\omega}$ signals. $I_{2\omega}$ is plotted on the left axis for the photon energy of $2\hbar\omega = 55$ eV (red circle), $2\hbar\omega = 57$ eV (blue circle), and $2\hbar\omega = 59$ eV (green circle) in the logarithmic scale. I_ω (orange circle) is plotted on the right axis for $\hbar\omega = 27.5$ eV. The dashed lines were fitted using a power law.

The absorption experiment was performed at the bending-magnet beam line (BL5B) [25] of UVSOR in Japan. The absorption spectra of the sample were recorded by the total-electron yield method at room temperature.

Figure 2(b) shows the absorption spectrum of the $GaFeO_3$ crystal. The features of Fe $3p$ absorption of $GaFeO_3$ are observed above 54 eV. Figure 2(c) shows the variation of the reflected intensity at a photon energy of $\hbar\omega = 27.5$ eV with respect to the incident intensity I_0. The dashed line represents fitting using the power law $\propto I_0^\beta$. The exponent coefficient is $\beta = 1.0$, which verifies the linearity of the ω component. The intensity of the 2ω component ($2\hbar\omega = 55$ eV) shows the apparent nonlinear dependence with I_0, as shown in Fig. 2(d). Moreover, the 2ω signal disappears when the photon energy is tuned to $2\hbar\omega = 53$ eV ($\hbar\omega = 26.5$ eV), which is below the Fe $3p$ absorption edge [Fig. 2(e)].

In Figure 3, $I_{2\omega}$ is plotted with respect to I_0 in the logarithmic scale with different photon energies. From the power-law fitting, the exponent coefficients are $\beta = 1.8$ ($2\hbar\omega = 55$ eV), $\beta = 2.0$ ($2\hbar\omega = 57$ eV), and $\beta = 2.0$ ($2\hbar\omega = 59$ eV). All of the fitting procedures are performed on the range of fundamental wave intensity, I_0, within $\pm 2\sigma$ determined by the Gaussian fitting to the histograms of I_0. The experimental values consistently match the quadratic intensity dependence ($\beta = 2$) of the SHG light. In order to compare the inclination of the data, I_ω for $\hbar\omega = 27.5$ eV is shown together. These results unambiguously indicate the detection of SHG light from the $GaFeO_3$ crystal.

Regarding the enhancement of SHG signals observed in Figs. 2(d) and 2(e), we discuss the feasibility of the

following double resonance scenario in the SHG process: (1) the ground state $|g\rangle$ is the high spin states of $3d^5$ and the first excitation state $|n'\rangle$ is $3d^6\underline{L}$, which is caused by the charge transfer from O $2s$ to Fe $3d$ state, where L expresses the ligand states of oxygen and the underline means the hole, (2) the second excitation state $|n\rangle$ is $3d^6 3p\underline{3p}$ that is resulted from the charge transfer from Fe $3p$ to O $2s$ state. SHG is emitted when $3d^6 3p\underline{3p}$ relaxes to initial $3d^5$ states. The transition from O $2s$ to Fe $3d$ state corresponds to the energy slightly lower than $\hbar\omega$ used in the experiments as shown in x-ray photoelectron spectroscopy measurement (see Fig. S1 in the Supplemental Material [26]). The transition from the Fe $3p$ to O $2s$ vacant state can occur when distribution of the Fe $3p$ states spreads over the O site. We performed the first-principles calculation for the local density of states (DOSs) in $GaFeO_3$. It is confirmed that O $2s$ state has a finite DOS at the Fe sites (see Fig. S2 in the Supplemental Material [26]). This implies that there is a tail of the O $2s$ wave function at the Fe site, resulting in a certain magnitude of matrix element between Fe $3p$ and O $2s$. This makes process (2) possible. For the generation of second harmonics, the IS breaking is indispensable, and it is a consequence of the summation over components with the dipole transitions. In the current energy range of Fe M edge, the SHG processes can be treated in a long-wavelength limit, which requires global IS breaking as well as the local one [26]. The double resonance condition gives the additional enhancement that apparently satisfies the first term in Eq. (1).

In order to further clarify the effect of double resonance, we conducted calculation for one of the second-order nonlinear susceptibility tensors, $\chi^{\mathrm{SHG}}_{zzz}$. In the point group of $GaFeO_3$, $\chi^{\mathrm{SHG}}_{zzz}$, $\chi^{\mathrm{SHG}}_{yzy}$, and $\chi^{\mathrm{SHG}}_{zyy}$ have a nonzero value in the second-order susceptibility tensor in the current setup, where x, y, and z are defined to be parallel with the a, b, and c crystal axis of $GaFeO_3$. Figure 4 shows the contribution of Fe $3p$ resonance to the $|\chi^{\mathrm{SHG}}_{zzz}|^2$ spectrum of $GaFeO_3$ near the Fe $3p$ edge. The horizontal axis denotes the energy of second harmonics. Both Fe $3p$ and O $2s$ resonance have been taken into account in the calculation. The details of the calculation are described in Sec. III of the Supplemental Material [26].

In Fig. 4(a), the experimental $I_{2\omega}$ values (green circles), which are normalized by $I_{2\omega}$ at 53 eV, are compared with the calculated $|\chi^{\mathrm{SHG}}_{zzz}|^2$ ones (red line), which reflect electronic states of $GaFeO_3$. As shown in the inset (i) of Fig. 4(b), the intermediate state is located slightly lower than the very medium point between the ground and excited states. The resonant enhancement at the Fe $3p$ edge is fairly reproduced by the calculation. This reinforces the scenario of the double resonance. Other second-order susceptibility tensor components, $\chi^{\mathrm{SHG}}_{yzy}$ and $\chi^{\mathrm{SHG}}_{zyy}$, are also expected to show the same behavior of resonance because this enhancement originates from the energy denominator as shown in Eq. (S1). We address the spectroscopic aspects of SHG measurements in the soft x-ray range. The calculated

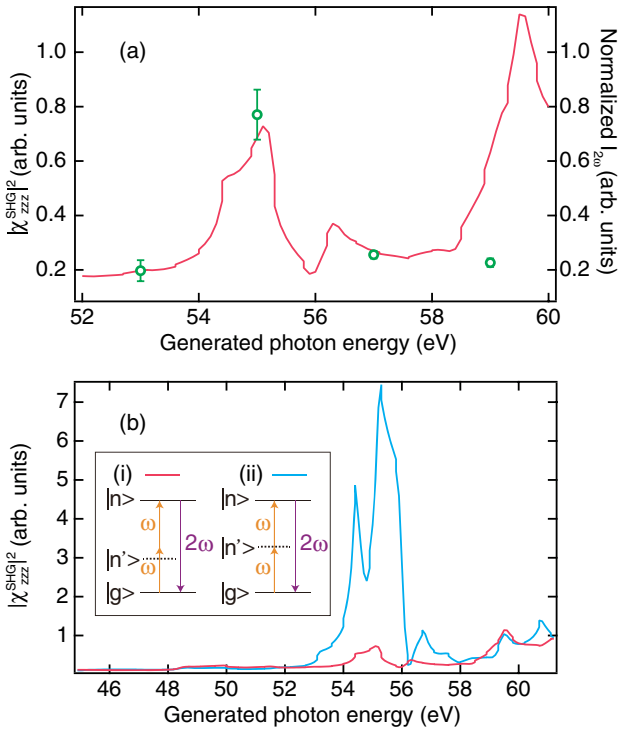

FIG. 4. The square of the second-order susceptibility tensor, $|\chi^{\mathrm{SHG}}_{zzz}|^2$, with respect to the photon energy of second harmonics near Fe $3p$ edge. The red and blue lines correspond to the transition process of the double resonance shown in the inset (i), the current case of $GaFeO_3$, and (ii) the ideal case, respectively. (a) Calculated $|\chi^{\mathrm{SHG}}_{zzz}|^2$ values (left) for (i) with the measured ones (right) (green circles) for $I_0 = 10$ μJ, that are normalized by $I_{2\omega}$ at 53 eV. (b) A comparison between the $|\chi^{\mathrm{SHG}}_{zzz}|^2$ values for the (i) and (ii) cases.

spectrum in Fig. 4(a) has a peak around 55 eV. This corresponds to the transition to the states on the Fermi level. The peaks shown in the higher photon energy range originated from the transition to the higher energy states than the Fermi level. It is of note that the deviation at 59 eV suggests that more theoretical work is necessary to consider $|\chi^{\mathrm{SHG}}|^2$ values in the post-edge region.

Finally, we discuss the element selectivity of the soft x-ray SHG. Figure 4(b) shows a comparison between the realistic case of $GaFeO_3$ [red, same as Fig. 4(a)] and the ideal configuration regarding the double resonance, inset (ii), where the intermediate state is located at the center of the ground and excited states. This suggests that the susceptibility tensor additionally increases by a factor of 10 when material satisfies the complete double resonant condition. In this ideal case, the inner-shell double resonance dominates over the interband transitions in the SHG process. This enables one to perform element-selective SHG spectroscopy in the soft x-ray range.

In summary, for the first time, we observed SHG in the reflected beam from a nonlinear crystal in the soft x-ray range. The SHG signals were enhanced by the double

resonant effect met by the transition between O $2s \rightarrow$ Fe $3d$ and between the Fe $3p \rightarrow$ O $2s$ state. In the SHG spectrum near the Fe $3p$ edge for $GaFeO_3$, there are contributions from the inner-shell double resonance at the $3p$-edge position and interband transitions that give a tail structure in the post-edge region. The theoretical calculation indicates that when the double resonance condition is fully met, the SHG signals are enhanced 10 times larger than that in the current system. The present method breaks the limitations regarding samples caused by the conventional transmission-type configuration in the NLO effect measurements in the EUV$\sim$ x-ray range. Furthermore, transition metal oxides make it possible to realize the double resonant condition due to the O L_1 and metal M edge, so that this resonant SHG scheme can be extended to a variety of samples, from strongly-correlated systems to the interfaces of heterojuctions in spintronics.

This work was partly supported by the MEXT program "X-Ray Free Electron Laser Priority Strategy Program" and by the Hyogo Science and Technology Association. We thank Masami Fujisawa, Takashi Tokushima, Mihoko Araki, and Yuka Kosegawa for their technical support. The measurement system was tested using facilities of the Synchrotron Radiation Research Organization, The University of Tokyo. We thank Goro Mizutani, Kenji Tamasaku, Yoshihiro Miyauchi, and Takanori Suzuki for valuable discussion about SHG. The XFEL experiments were performed at the BL1 of SACLA with the approval of the Japan Synchrotron Radiation Research Institute (JASRI) (Proposal No. 2016B8078). The XPS measurement was conducted at the BL-2A of Photon Factory (Proposal No. 2016G602). Sh. Y. was supported by the Grant-in-Aid for JSPS Fellows and the Program for Leading Graduate Schools (MERIT).

*imatsuda@issp.u-tokyo.ac.jp
†Present address: Dresden High Magnetic Field Laboratory (HLD-EMFL), Helmholtz-Zentrum Dresden-Rossendorf, D-01328 Dresden, Germany.

[1] R. W. Boyd, *Nonlinear Optics* (Academic Press, New York, 2008).
[2] M. Kauranen and A. V. Zayats, Nat. Photonics **6**, 737 (2012).
[3] P. Pantazis, J. Maloney, D. Wu, and S. E. Fraser, Proc. Natl. Acad. Sci. U.S.A. **107**, 14535 (2010).
[4] K. L. Seyler, J. R. Schaibley, P. Gong, P. Rivera, A. M. Jones, S. Wu, J. Yan, D. G. Mandrus, W. Yao, and X. Xu, Nat. Nanotechnol. **10**, 407 (2015).
[5] Y. R. Shen, *Fundamentals of Sum-Frequency Spectroscopy* (Cambridge Molecular Science, Cambridge, 2016).
[6] *Nonlinear Optics, Quantum Optics, and Ultrafast Phenomena with X-Rays*, edited by B. Adams (Kluwer Academic, Dordrecht, 2003).
[7] R. M. Corn and D. A. Higgins, Chem. Rev. **94**, 107 (1994).
[8] H. Liu, Y. Li, Y. S. You, S. Ghimire, T. F. Heinz, and D. A. Reis, Nat. Phys. **13**, 262 (2017).
[9] N. Ishii, K. Kaneshima, K. Kitano, T. Kanai, S. Watanabe, and J. Itatani, Nat. Commun. **5**, 3331 (2014).
[10] T. T. Luu, M. Garg, S. Y. Kruchinin, A. Moulet, M. T. Hassan, and E. Goulielmakis, Nature (London) **521**, 498 (2015).
[11] F. Bencivenga, R. Cucini, F. Capotondi, A. Battistoni, R. Mincigrucci, E. Giangrisostomi, A. Gessini, M. Manfredda, I. P. Nikolov, E. Pedersoli *et al.*, Nature (London) **520**, 205 (2015).
[12] T. E. Glover, D. M. Fritz, M. Cammarata, T. K. Allison, S. Coh, J. M. Feldkamp, H. Lemke, D. Zhu, Y. Feng, R. N. Coffee *et al.*, Nature (London) **488**, 603 (2012).
[13] S. Shwartz, M. Fuchs, J. B. Hastings, Y. Inubushi, T. Ishikawa, T. Katayama, D. A. Reis, T. Sato, K. Tono, M. Yabashi, S. Yudovich, and S. E. Harris, Phys. Rev. Lett. **112**, 163901 (2014).
[14] M. Yabashi and H. Tanaka, Nat. Photonics **11**, 12 (2017).
[15] T. Ishikawa *et al.*, Nat. Photonics **6**, 540 (2012).
[16] G. New, *Introduction to Nonlinear Optics* (Cambridge University Press, Cambridge, 2011).
[17] Y. R. Shen, *The Principles of Nonlinear Optics* (John Wiley & Sons, New York, 1984).
[18] S. Owada, K. Togawa, T. Inagaki, T. Hara, T. Tanaka, Y. Joti, T. Koyama, K. Nakajima, H. Ohashi, Y. Senba *et al.*, J. Synchrotron Radiat. **25**, 282 (2018).
[19] C. Martin and S. Bowyer, Appl. Opt. **21**, 4206 (1982).
[20] M. Hirata, T. Cho, E. Takahashi, N. Yamaguchi, T. Kondoh, K. Matsuda, S. Aoki, K. Tanaka, H. Maezawa, and S. Miyoshi, Nucl. Instrum. Methods Phys. Res., Sect. B **66**, 479 (1992).
[21] T. Arima, J. Phys. Condens. Matter **20**, 434211 (2008).
[22] Y. Ogawa, Y. Kaneko, J. P. He, X. Z. Yu, T. Arima, and Y. Tokura, Phys. Rev. Lett. **92**, 047401 (2004).
[23] M. Rumi and J. W. Perry, Adv. Opt. Photonics **2**, 451 (2010).
[24] K. Tamasaku, E. Shigemasa, Y. Inubushi, T. Katayama, K. Sawada, H. Yumoto, H. Ohashi, H. Mimura, M. Yabashi, K. Yamauchi, and T. Ishikawa, Nat. Photonics **8**, 313 (2014).
[25] M. Sakurai, S. Morita, J. Fujita, H. Yonezu, K. Fukui, K. Sakai, E. Nakamura, M. Watanabe, E. Ishiguro, and K. Yamashita, Rev. Sci. Instrum. **60**, 2089 (1989).
[26] See Supplemental Material at http://link.aps.org/supplemental/10.1103/PhysRevLett.120.223902, for x-ray photoelectron spectroscopy, the density of states calculated by the first principle calculation, the detail of SHG calculation and the relation between the inversion-symmetry breaking and Fe $3p$ core hole.